APL MATERIALS **2**, 076104 (2014)

Role of surface states and defects in the ultrafast nonlinear optical properties of CuS quantum dots

K. A. Ann Mary,[1] N. V. Unnikrishnan,[1,a] and Reji Philip[2]
[1]*School of Pure and Applied Physics, Mahatma Gandhi University, Kottayam 686560, India*
[2]*Light and Matter Physics Group, Raman Research Institute, C.V. Raman Avenue, Sadashivanagar, Bangalore 560080, India*

(Received 4 April 2014; accepted 20 June 2014; published online 1 July 2014)

We report facile preparation of water dispersible CuS quantum dots (2–4 nm) and nanoparticles (5–11 nm) through a nontoxic, green, one-pot synthesis method. Optical and microstructural studies indicate the presence of surface states and defects (dislocations, stacking faults, and twins) in the quantum dots. The smaller crystallite size and quantum dot formation have significant effects on the high energy excitonic and low energy plasmonic absorption bands. *Effective* two-photon absorption coefficients measured using 100 fs laser pulses employing open-aperture Z-scan in the plasmonic region of 800 nm reveal that CuS quantum dots are better ultrafast optical limiters compared to CuS nanoparticles. [http://dx.doi.org/10.1063/1.4886276]

Semiconductor nanoparticles (NPs) are promising candidates for solar and photovoltaic cells,[1,2] optical data storage,[3] and nonlinear optics[4–7]owing to their enhanced and tunable optical properties. In particular, near-infrared (NIR) plasmonic effects in semiconductor NPs are emerging as a subject of active research because of their potential applications in photonic devices. While metallic nanostructures of Au[8,9] and Ag[10] are well known plasmonic materials for the visible region with applications in photovoltaics, sensing, and tissue imaging, doped semiconductor nanostructures[11] are important for NIR plasmonics with a significant role in NIR detectors[12] and deep tissue imaging.[13] However, the nonlinear optical properties of semiconductor nanomaterials having NIR plasmonic applications are not well explored yet.

Among semiconducting nanoparticles, transition metal chalcogenides stand out for the reason that they can form variety of stoichiometric compounds with variable optical band gaps. Copper chalcogenides are known to exhibit NIR absorption and localized surface plasmon resonances (SPR). CuS is an intermediate compound having a strong NIR absorption due to self doped p-type carriers, having potential applications in photocatalytic activity,[14] DNA sensing,[15] and photothermal therapy.[16] Though CuS nanocrystals with different morphologies can be prepared using various capping agents,[16–18] detailed investigations of the crystal growth process, microstructural defects, optical properties, and ultrafast nonlinear optical properties of the cubic–hexagonal phase of CuS quantum dots (QDs) are not readily available in literature. Considering the photonic applications of semiconductor plasmonic materials, in addition to exploring their SPR properties, it is crucial to understand how the nonlinear optical properties evolve from quantum dots to nanoparticles. Therefore, systematic investigations of their preparation, microstructural defects, and crystalline, optical and nonlinear optical properties are desired. In this background, in the present article we report the synthesis of CuS QDs (2–4 nm) and NPs (5–11nm) through a soft chemical route, by using polyvinylpyrolidine (PVP) as the capping agent. Their structural, crystalline, and optical properties are investigated in detail and the dependence of NIR absorption on the surrounding solvent medium is studied. We also investigate the mechanism and efficiency of ultrafast (100 fs laser pulses)

[a]Author to whom correspondence should be addressed. Electronic mail: nvu100@yahoo.com

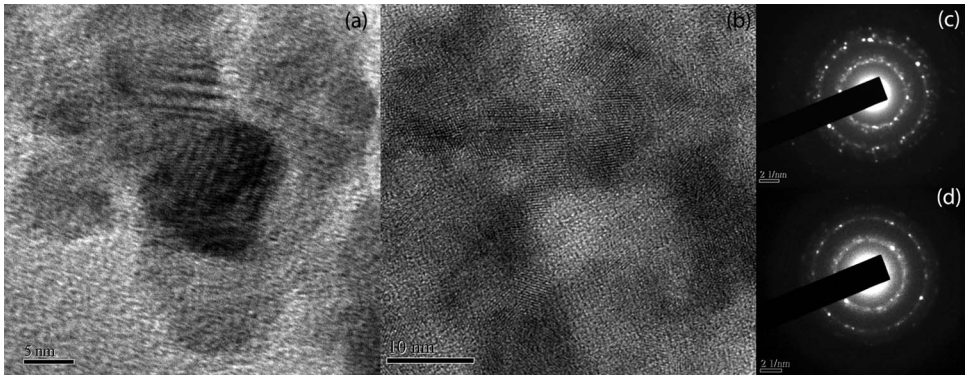

FIG. 1. HRTEM images and SAED patterns of CuS–PVP NPs (a) and (c) and QDs (b) and (d).

nonlinear optical absorption of CuS QDs and NPs using open aperture Z-scan at the near-resonant SPR wavelength of 800 nm.

Synthesis of CuS QDs was carried out with PVP and copper acetate as starting materials. We added 0.2 M copper acetate to 0.5 mM PVP solution in distilled water under magnetic stirring. The mixture was heated to 70 °C and kept for 30 min with constant stirring to get a homogenous solution. Aqueous solution of 0.2 M thiourea was added to the mixture in drops. Addition of this sulfur precursor into the mixture led to immediate sequential color changes through green, dark green, dark brown, and finally black. The reaction was maintained at 70 °C for 1 h before cooling to room temperature. The solid precipitate obtained was separated by centrifugation. It was washed several times with distilled water and ethanol to remove impurities and excess capping agents, and finally dried overnight in a hot air oven at 50 °C. The reaction procedure for CuS nanoparticles is similar to that for CuS QDs except that the sulfur precursor used is thioacetamide. The synthesis of the CuS–PVP nanocrystals is similar to the method reported previously for metal sulfide nanoparticles such as PbS,[19] ZnS,[20] and CuS.[21]

UV-VIS-NIR absorption spectra were measured using a Varian Cary 5000 spectrophotometer. Transmission electron micrographs (TEM) and selected area electron diffraction (SAED) patterns acquired from a JEOL JEM 2100 electron microscope were used to determine the morphological and crystalline nature of the products. X-ray diffraction patterns were obtained from PANalytical X'Pert PRO X-ray diffractometer.

Nonlinear optical properties were investigated using the ultrafast open-aperture Z-scan technique,[22] employing 100 fs laser pulses at 800 nm from a regeneratively amplified Ti:Sapphire laser for excitation (TSA-10, *Positive Light*). Samples dispersed in distilled water were taken in a 1 mm quartz cuvette, and mounted on a stepper motor controlled translation stage. The incident laser pulse energy was set to a suitable low value of 10 μJ by inserting a set of neutral density filters. Laser pulses were focused using a converging lens and samples were scanned along the beam axis through the beam focus. The transmitted energy as a function of the sample position was measured using a pyroelectric energy detector (Rjp735, Laser Probe Corp.) placed in the far field. Laser was run at a repetition rate of 10 Hz for energy stability, but the experiment was in effect done in the single-shot mode by using a synchronized fast mechanical shutter in the beam path, which could allow single pulses from the pulse train to pass through as desired. The experiment was automated using a LabVIEW program.

As CuS can exist in various crystalline phases which are structurally close with similar lattice parameters, an exact structural analysis of the prepared materials is essential. The crystal structure and morphology can be elucidated from SAED patterns (Figure 1) and transmission electron micrograph (TEM) images shown in Figure s1 of the supplementary material.[23] For QDs, the size of the nanocrystallites is in the range of 2–4 nm, while for NPs, the average particle size is in the range of 5–11 nm. The SAED patterns obtained for NPs match well with the hexagonal CuS structure, with prominent rings corresponding to diffraction peaks of (102), (103), (006), (110), (108), and (116) planes with the corresponding d-spacings as 3.046 Å, 2.871 Å, 2.718 Å, 1.868 Å, 1.718 Å, and 1.535

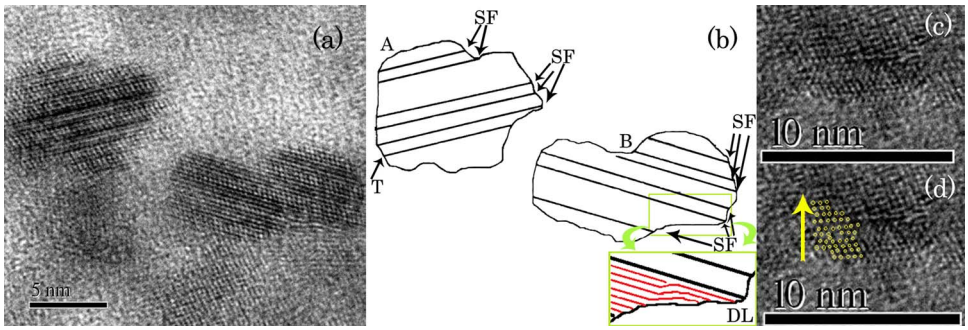

FIG. 2. HRTEM image of CuS-PVP QDs showing abrupt edges (a). Dislocations, twins, and stacking faults are illustrated in (b). A twin region formed between the cubic and hexagonal phases of CuS is illustrated in (c) and (d). The stacking sequence is determined as ABCABABCAB in the direction indicated by the arrow.

Å, respectively (ICDD No. 65–3561). For QDs the d-spacings of 3.117 Å, 1.917 Å, and 1.589 Å obtained from the SAED pattern are consistent with the (111), (200), and (311) lattice planes of the face centered cubic phase of CuS (ICDD No. 89-2073). The occurrence of a prominent ring with d = 2.810 Å corresponds to the (103) hexagonal plane in addition to cubic CuS. The position and relative intensities of the diffraction peaks obtained from powder XRD are also compared with corresponding ICDD patterns. Detailed explanation is included in Figure s2 of the supplementary material.[23]

HRTEM images of CuS NPs and QDs are shown in Figures 1(a) and 1(b), respectively. The corresponding HRTEM images (Figures 1(c) and 1(d)) reveal that while QDs show randomly oriented crystallites with sharp edges, NPs exhibit spherical shapes and smooth edges. The darker region of the observed image results from the thickness variation of overlapped (102) and (103) hexagonal lattice planes of the NPs. As clearly seen from the HRTEM image, the grains stacked over one another with different interplanar distances give rise to modulated fringes known as Moire interference. This effect has been previously observed in hexagonal CuS nanodisks,[24] graphene,[25] and silicon.[26] In addition to the occurrence of grain boundaries, CuS QDs possess a considerable number of planar defects which can be seen from Figure 2. The nanocrystal shown in Figure 2(a) does not have a definite shape but has abrupt edges, similar to many nanocrystals in the sample which contain dislocations (DL), twins (T), and stacking faults (SF). Details are illustrated in Figure 2(b). While nanocrystal A consists of many stacking faults and a twin boundary, nanocrystal B contains edge dislocations and stacking faults. These defects are the active sites for the nonradiative recombination of absorbed radiation.

From the SAED patterns it is evident that CuS QDs consist of both cubic and hexagonal phases suggesting the possible formation of wide variety of microstructures. Wherever the cubic arrangement ABCABC or the hexagonal stacking sequence ABABAB is disrupted by the introduction of a new layer or the absence of a layer, a stacking fault (ABCABABC) is created. If it does not correct itself immediately and continues over a few more atomic spacings, a twin defect is formed. A twin region formed between the cubic and hexagonal phases of CuS is illustrated in Figures 2(c) and 2(d). The close-packed-layer-stacking sequence is determined as ABCABABCAB as indicated by the arrow.

The formation of dislocations, twins, and stacking faults are often direct consequences of oriented attachment (OA) based crystal growth. The surface features of CuS QDs depict the fact that several primary particles act as building blocks, whose aggregation by sharing a common crystallographic orientation results in the development of QDs with irregular shapes. Under hydrothermal treatment, crystal growth occurs through collision and coalescence involving primary particles and secondary particles or multilevel particles. The reduction in surface energy due to the removal of nanocrystal interfaces acts as the driving force for the mechanism to continue. This is similar to that reported earlier for H_2O–ZnS and mercaptoethanol-capped ZnS samples.[27,28] At the same time, CuS NPs are almost spherical in shape with smooth edges, and do not have any dislocations and planar

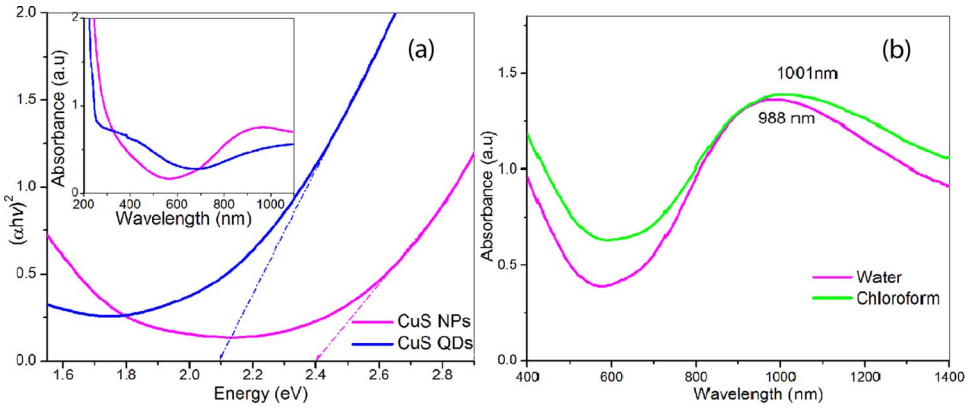

FIG. 3. (a) Tauc plots calculated from the absorption spectra (inset) of CuS-PVP QDs and NPs in distilled water. (b) SPR observed from the absorption spectra in water and chloroform as solvents.

defects. This suggests that the crystal growth mechanism is possibly classical Ostwald ripening (OR) in which larger particles grow at the expense of smaller particles. The coalescence of particles often happens through the accumulation of ions on to the particle surface from the solution, and the driving force for this growth mechanism is the reduction in the total surface free energy. The crystal growth of hydrothermally treated PbS nanoparticles, for instance, is reported to occur through the Ostwald ripening mechanism.[29]

The synthesis conditions are similar for both QDs and NPs in terms of the temperature, duration of the reaction, surface adsorption of anions (Ch_3COO^-), capping ligands, and concentration. The difference is in the source of sulfur, which seems to be the crucial factor for OA during crystal growth. Addition of copper ions into an aqueous solution of PVP results in the formation of the Cu-PVP complex, through donor-acceptor interactions from the unshared electron pairs of –O– and N– of the PVP chain to the Cu ions. Thiourea used for preparing CuS QDs has two amine groups and hence it can be effectively adsorbed, whereas CuS NPs are prepared from thioacetamide which has a methyl group instead of the amine groups. The decomposition of thiourea is faster in the presence of Cu ions[30] and the metal removes sulfide as metal sulfide from the Cu-PVP complex. These strongly capped primary particles undergo OA crystal growth at suitable crystallographic phases. On the contrary, thioacetamide is an efficient sulfur donor and tends to release sulfide ions directly in the solution by hydrolysis.[30] The free sulfide ions react directly with the copper species in the solution to form CuS nanocrystals. Crystal growth continues through the OR mechanism by the accumulation of ions on to the particle surface.

The steady state absorption spectrum of CuS measured in distilled water exhibits a 300–500 nm absorption band which is slightly blueshifted from the bulk band gap due to quantum confinement effects (inset of Figure 3(a)). This low energy absorption peak arises from the $1S_h$-$1S_e$ excitonic transition found in semiconductor nanoparticles. From the Tauc plot obtained by the extrapolation of $(\alpha h\nu)^2$ versus $h\nu$, the band gaps of the NPs and QDs are calculated to be 2.4 eV and 2.1 eV, respectively (Figure 3(a)). The slight increase observed in the band gap energy of NPs compared to the values reported in literature can be attributed to quantum confinement effects.[18] The presence of surface states and traps in and around the band gap of the densely capped CuS–PVP QDs can be the reason for the lower band gap of the QDs. Different stoichiometric phases of $Cu_{2-x}S$ QDs have characteristic absorption bands, and the observed absorption band corresponds to pure covellite CuS.

In addition to these excitonic features, CuS also exhibits a SPR mode in the near-infrared range. Evolution of this NIR band is related to copper vacancies which contribute to free carrier absorption from excess holes in the valence band. The spectral properties of copper chalcogenide nanocrystals in the NIR region showing carrier concentration dependent plasmonic absorption, and the possible non-stoichiometry between copper and sulfur, have been studied in detail by Zhao *et al.*[31,32] Wavelength tuning of the SPR mode has been previously achieved by actively controlling carrier density concentrations by varying the size, shape, and stoichiometry of the $Cu_{2-x}S$

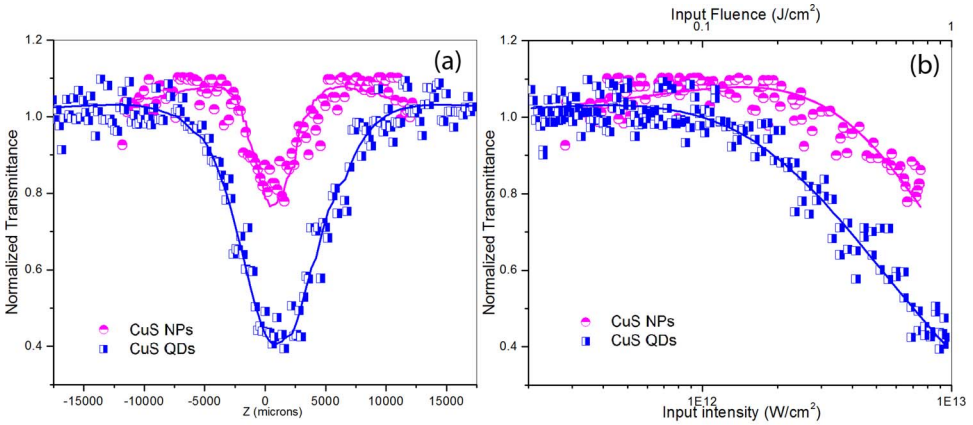

FIG. 4. Open aperture Z-scan curves measured in CuS-PVP QDs and NPs for excitation by ultrafast (100 fs) laser pulses at the SPR wavelength of 800 nm (a). Nonlinear transmission as a function of input intensity and fluence, calculated from the Z-scan curves (b). While QDs exhibit a predominantly optical limiting behavior, NPs exhibit absorption saturation at moderate input intensities followed by limiting at the higher intensities.

nanocrystallites.[33,34] In addition to the size, shape, and stoichiometry dependence of this NIR signature, the surrounding dielectric medium also has an influence on the plasmonic behavior of the nanocrystals. For typical plasmonic behavior, the absorption band will be blueshifted when the refractive index of the surrounding medium decreases. To examine the effect of the solvent on the SPR band, we compared the absorption spectra of CuS-PVP measured in water (refractive index 1.33) with that measured in chloroform (refractive index 1.44). The band shifts to a higher wavelength for CuS/chloroform owing to its higher refractive index, in accordance with the findings of Luther *et al.*[18]

Ultrafast nonlinear transmission measurements in CuS-PVP QDs and NPs were conducted using laser pulses of 100 fs duration at the excitation wavelength of 800 nm, which is in the NIR plasmonic absorption regime. Results obtained from open aperture Z-scan measurements are shown in Figure 4(a). Samples used were dispersed in distilled water to the appropriate dilution so that when taken in 1 mm cuvettes the linear transmission was 75% at 800 nm. The two peaks seen in the Z-scan of CuS NPs (flanking the central valley) indicate absorption saturation, whereas the valleys seen for both QDs and NPs indicate reverse saturation. Nonlinear transmission as a function of input intensity and fluence, calculated from the Z-scan data, is plotted in Figure 4(b). Both Z-scans exhibit valleys with reduced normalized transmission near the beam focus, indicating optical limiting behavior at the higher intensities used.

Absorptive optical nonlinearity in metal and semiconductor nanomaterials excited by ultrafast laser pulses mostly arise from saturable absorption (SA), multiphoton absorption, and free carrier absorption (FCA). We find that the best numerical fits to the measured Z-scan data can be obtained by considering a nonlinear absorption coefficient $\alpha(\mathrm{I})$ that includes saturable absorption, free carrier absorption, and two-photon absorption, as given by the equation

$$\alpha(I) = \frac{\alpha_0}{1 + \left(\frac{I}{I_s}\right)} + \mathrm{N_c(I)}\sigma_c \mathrm{I} + \beta I, \tag{1}$$

where α_0 is the linear absorption coefficient, I is the input intensity, $\mathrm{I_s}$ is the saturation intensity, Nc(I) is the intensity-dependent carrier density, σ_c is the free carrier absorption cross section, and β is the two-photon absorption coefficient. The product of $\mathrm{N_c(I)}$ with σ_c can be written as β_c (I), which is the free carrier absorption coefficient. Considering a net *effective* nonlinear absorption coefficient β_{eff} (I) given by $\beta + \beta_c$ (I), the normalized transmittance can be obtained by numerically solving the propagation equation

$$\frac{dI}{dz'} = -\left[\left(\alpha_0 \Big/ \left(1 + \frac{I}{I_s}\right)\right) + \beta_{eff}(I)I\right] I, \tag{2}$$

where z′ is the propagation distance within the sample. From the best numerical fits to the experimental data, the saturation intensity I_s and the *effective* nonlinear absorption coefficient β_{eff} are calculated to be 1.0×10^{16} W/m^2 and 2.3×10^{-14} m/W for CuS QDs, and 2.0×10^{16} W/m^2 and 6.0×10^{-15} m/W for CuS NPs, respectively. It may be noted that β_{eff} is an order of magnitude larger in CuS QDs compared to the NPs, which makes the QDs better optical limiters. Similar size dependence in the optical limiting behavior and efficiency of nanoparticles and atomic nanoclusters of Au has been reported recently.[8]

The mechanism behind ultrafast optical limiting in the present case is two-photon absorption acting along with free carrier absorption. The two-photon energy of 3.1 eV for 800 nm excitation is greater than the band gap energy of CuS QDs and NPs. The band structure of CuS is such that the valence band maximum is formed from occupied S 3*p* and Cu 3*d* states whereas the conduction band minimum is formed from unoccupied Cu 4*p* states.[35] QDs being ultra small particles, a large percentage of atoms are present on or near the surfaces. Furthermore, the presence of infinite interfaces between the QD and its surroundings and the occurrence of imperfect surfaces from OA crystal growth often create electron and/or hole traps.[36] Anand *et al.*[37] have shown that the formation of surface states and traps in and around the band edge in a system is conducive for nonlinear absorption. Moreover, the NIR band formed in response to the oxidative environment generates an additional level from unoccupied 3*d*-4*s* orbitals of Cu^{II}, at an energy of 1.1 eV above the valence band, which has an electron acceptor character.[35] The higher β_{eff} and limiting efficiency of CuS QDs indicate a higher concentration of defect levels and surface states.

On the other hand, in CuS NPs the plasmon band is stronger compared to that in QDs, and absorption saturation is seen at moderate intensities as indicated by the two humps flanking the valley in the Z-scan curves. Absorption saturation associated with SPR in metallic nanoparticles has been reported before.[8,38] Generally SPR will decay through the channels of radiative emission, interband excitation, and intraband excitation. As CuS has no radiative emission around 800 nm (1.55 eV) and interband transition requires a relatively higher energy of 2.3 eV, plasmon excitation decays mainly through intraband excitation generating more free carriers. In addition, excess holes will be generated in the valence band due to the copper vacancies (copper vacancy density increases with size, possibly due to the reducing surface/volume ratio[18]). Thus the saturation of one photon absorption due to the presence of SPR, as well as the subsequent decrease in transmission due to free carrier absorption, can both be seen in CuS NPS. As discussed earlier, the higher density of defects and surface traps renders a higher optical limiting efficiency for CuS QDs.

It may be noted that while the present Z-scan measurements have been carried out only at the peak output wavelength of a typical ultrafast Ti:Sapphire laser, it is possible to measure the nonlinear spectrum over a broad wavelength range if a tunable laser is used. Interestingly, the nonlinear absorption spectra need not show any simple relation with the one-photon spectra: for instance, it has been reported that the maxima of nonlinear absorption do not correspond to the absorption edge in the one-photon absorption spectrum for $CuInS_2$,[39] CdSe,[5] and CdS[40] samples.

In summary, we have prepared PVP capped CuS nanoparticles and QDs which are highly dispersible in water, through a nontoxic, green, one-pot synthesis method. Dispersibility in water makes the QDs and NPs relevant for biological applications and *in vivo* imaging. The morphology, microstructural defects, and internal crystallinity are confirmed from TEM and HRTEM studies. A pure hexagonal phase of CuS is observed in the NPs, whereas the coexistence of cubic and hexagonal phases is seen in the QDs. In addition to grain boundaries, CuS QDs exhibit considerable amount of dislocations and planar defects such as twins and stacking faults. Growth process for CuS QDs is dominated by oriented attachment (OA) based crystal growth at suitable crystallographic phases, whereas for CuS NPs, crystal growth continues through the classical Ostwald ripening mechanism by accumulation of ions. Optical absorption in the linear as well as nonlinear regimes is examined for both QDs and NPs. The lower band gap energy in CuS QDs suggests the existence of electron/hole traps. The presence of defects and surface traps enhances free carrier absorption in CuS QDs resulting in a relatively higher optical limiting efficiency compared to the NPs.

[1] V. Gupta, N. Chaudhary, R. Srivastava, G. D. Sharma, R. Bhardwaj, and S. Chand, J. Am. Chem. Soc. **133**, 9960 (2011).
[2] J. Bang, J. Park, J. H. Lee, N. Won, J. Nam, J. Lim, B. Y. Chang, H. J. Lee, B. Chon, and J. Shin, Chem. Mater. **22**, 233 (2010).

[3] T. Shiono, H. Yamamoto, and S. Nishino, Jpn. J. Appl. Phys. **43**, 4941 (2004).
[4] N. Venkatram, R. Sathyavathi, and D. N. Rao, Opt. Express **15**, 12258 (2007).
[5] M. Nyk, D. Wawrzynczyk, J. Szeremeta, and M. Samoc, Appl. Phys. Lett. **100**, 041102 (2012).
[6] I. L. Bolotin, D. J. Asunskis, A. M. Jawaid, Y. Liu, P. T. Snee, and L. Hanley, J. Phys. Chem. C **114**, 16257 (2010).
[7] A. D. Lad, P. Premkiran, G. R. Kumar, and S. Mahamuni, Appl. Phys. Lett. **90**, 133113 (2007).
[8] R. Philip, P. Chantharasupawong, H. Qian, R. Jin, and J. Thomas, Nano Lett. **12**, 4661 (2012).
[9] K. Lee and M. A. El-Sayed, J. Phys. Chem. B **110**, 19220 (2006).
[10] K. J. Lee, P. D. Nallathamby, L. M. Browning, C. J. Osgood, and X. N. Xu, ACS Nano **1**, 133 (2007).
[11] L. Chou, N. Shin, S. V. Sivaram, and M. A. Filler, J. Am. Chem. Soc. **134**, 16155 (2012).
[12] L. Colace, G. Masini, F. Galluzzi, G. Assanto, G. Capellini, L. Di Gaspare, E. Palange, and F. Evangelisti, Appl. Phys. Lett. **72**, 3175 (1998).
[13] X. Liu, C. Lee, W. Law, D. Zhu, M. Liu, M. Jeon, J. Kim, P. N. Prasad, C. Kim, and M. T. Swihart, Nano Lett. **13**, 4333 (2013)
[14] C. Ratanatawanate, A. Bui, K. Vu, and K. J. Balkus, Jr., J. Phys. Chem. C. **115**, 6175 (2011).
[15] S. Zhang, H. Zhong, and C. Ding, Anal. Chem. **80**, 7206 (2008).
[16] Y. Li, W. Lu, Q. Huang, M. Huang, C. Li, and W. Chen, Nanomedicine **5**, 1161 (2010).
[17] B. Li, Y. Xie, and Y. Xue, J. Phys. Chem. C **111**, 12181 (2007).
[18] J. M. Luther, P. K. Jain, T. Ewers, and A. P. Alivisatos, Nat. Mater. **10**, 361 (2011).
[19] A. A. Patel, F. Wu, J. Z. Zhang, C. L. Torres-Martinez, R. K. Mehra, Y. Yang, and S. H. Risbud, J. Phys. Chem. B **104**, 11598 (2000).
[20] A. Silambarasan, H. P. Kavitha, S. Ponnusamy, M. Navaneethan, and Y. Hayakawa, Mater. Lett. **81**, 209 (2012).
[21] A. Dutta and S. K. Dolui, Mater. Chem. Phys. **112**, 448 (2008).
[22] M. Sheik-Bahae, A. A. Said, T. M. Wei, D. J. Hagan, and E. W. Van Stryland, IEEE J. Quant. Electron. **26**, 760 (1990).
[23] See supplementary material at http://dx.doi.org/10.1063/1.4886276 for transmission electron micrograph (TEM) images (Figure s1) and detailed explanation of XRD analysis (Figure s2).
[24] J. S. Cruz, S. A. M. Hernández, F. P. Delgado, O. Z. Angel, R. C. Pérez, and G. T. Delgado, Int. J. Photoenergy **2013**, 178017 (2013).
[25] J. H. Warner, M. H. Rümmeli, T. Gemming, B. Büchner, and A. D. Briggs, Nano Lett. **9**, 102 (2009).
[26] F. J. Lopez, E. R. Hemesath, and L. J. Lauhon, Nano Lett. **9**, 2774 (2009).
[27] F. Huang, H. Zhang, and J. F. Banfield, J. Phys. Chem. B **107**, 10470 (2003).
[28] F. Huang and J. F. Banfield, J. Am. Chem. Soc. **127**, 4523 (2005).
[29] X. Zhao, I. Gorelikov, S. Musikhin, S. Cauchi, V. Sukhovatkin, E. H. Sargent, and E. Kumacheva, Langmuir **21**, 1086 (2005).
[30] G. Hodes, *Chemical Solution Deposition of Semiconductor Films* (CRC Press, 2002).
[31] Y. Zhao, H. Pan, Y. Lou, X. Qiu, J. Zhu, and C. Burda, J. Am. Chem. Soc. **131**, 4253 (2009).
[32] Y. Zhao and C. Burda, Energy Environ. Sci. **5**, 5564 (2012).
[33] I. Kriegel, C. Jiang, J. Rodríguez-Fernández, R. D. Schaller, D. V. Talapin, E. da Como, and J. Feldmann, J. Am. Chem. Soc. **134**, 1583 (2012).
[34] S. Hsu, W. Bryks, and A. R. Tao, Chem. Mater. **24**, 3765 (2012).
[35] M. V. Artemyev, V. S. Gurin, K. V. Yumashev, P. V. Prokoshin, and A. M. Maljarevich, J. Appl. Phys. **80**, 7028 (1996).
[36] Y. Wang and N. Herron, J. Phys. Chem. **95**, 525 (1991).
[37] B. Anand, S. R. Krishnan, R. Podila, S. S. Sankara Sai, A. M. Rao, and R. Philip, Phys. Chem. Chem. Phys. **16**, 8168 (2014).
[38] R. Philip, G. Ravindra Kumar, N. Sandhyarani, and T. Pradeep, Phys. Rev. B. **62**, 13160 (2000).
[39] B. Cichy, D. Wawrzynczyk, A. Bednarkiewicz, M. Samoc, and W. Strek, Appl. Phys. Lett. **102**, 243702 (2013).
[40] J. Szeremeta, M. Nyk, D. Wawrzynczyk, and M. Samoc, Nanoscale **5**, 2388 (2013).